Catal Lett (2012) 142:882–888
DOI 10.1007/s10562-012-0844-y

Role of the Support and the Ru Precursor on the Performance of Ru/Carbon Catalysts Towards H_2 Production Through $NaBH_4$ Hydrolysis

Carmelo Crisafulli · Salvatore Scirè · Roberta Zito · Corrado Bongiorno

Received: 23 February 2012 / Accepted: 13 May 2012 / Published online: 26 May 2012

Abstract This paper details $NaBH_4$ hydrolysis over Ru catalysts supported on activated carbons of different origin and morphology. The influence of two Ru precursors [$RuCl_3$ or $Ru(NO)(NO_3)_3$] was also investigated. It was found that the H_2 production rate strongly depends both on the support characteristics and the Ru precursor, the best performance being obtained using an activated carbon of vegetable origin as the support and $Ru(NO)(NO_3)_3$ as the precursor. It was concluded that the carbon type and the Ru precursor mutually affect the size of the supported Ru nanoparticles with the best combination being the one leading to Ru particles with diameters around 2.5 nm, which is regarded as optimal for $NaBH_4$ hydrolysis.

Keywords Fuel cells · Hydrogen on demand · Sodium borohydride · Ruthenium · Alkali metals · Structure sensitive reaction

1 Introduction

The Proton exchange membrane fuel cell (PEMFC) using hydrogen as fuel is considered one of the most promising alternatives to combustion engines due to its zero emissions [1]. In order to operate a PEMFC successfully, a safe and convenient hydrogen storage and production system is required [1, 2]. The development of a hydrogen economy (production, storage, distribution and consumption) is today quite difficult due to hydrogen flammability and storage problems [2]. A stabilized aqueous solution of metal hydride is considered an appropriate material for hydrogen storage and regarded as an ideal source of pure hydrogen for fuel cell applications. Diverse metal hydrides were studied, such as LiH, CaH_2, MgH_2, $NaBH_4$ and $LiAlH_4$ [3–5]. Among these, sodium borohydride is the preferred option due to its high hydrogen storage capacity (10.8 wt%), non-flammability of its aqueous solution and ability to control hydrogen production. Moreover it is economically feasible in comparison to other hydrides [6–12].

The $NaBH_4$ hydrolysis ($NaBH_4 + 2H_2O \rightarrow NaBO_2 + 4H_2$) is an exothermic reaction releasing 217 kJ mol^{-1} of $NaBH_4$ [13]. It can occur from 0 °C, releasing a non-toxic by-product such as sodium metaborate ($NaBO_2$) [14, 15]. The self–hydrolysis reaction is inhibited by keeping $NaBH_4$ solutions at pH >13. At this pH, hydrogen release occurs only in the presence of specific catalysts, allowing the development of "hydrogen on demand" systems (HOD) [13, 16, 17]. Numerous catalysts have been investigated for $NaBH_4$ hydrolysis, with special attention devoted to heterogeneous catalysts based on Ru [6, 7, 16, 18–24], Co [25–30], Pt [9–11, 31, 32], Ni [33–35] and Pd [16, 36, 37]. Ni and Co catalysts have attracted considerable interest due to their lower cost compared to noble metals, whereas Ru is preferred for HOD applications despite its high price due to its elevated activity.

The choice of the support and the metal precursor can have a key role in the optimization of the catalytic performance of supported metal catalysts. The support can directly take part in the reaction mechanism favoring the adsorption/desorption of the reactants/products on/by the catalytic system, or it can influence the dispersion of

C. Crisafulli · S. Scirè (✉) · R. Zito
Dipartimento Scienze Chimiche, Università di Catania, Viale A. Doria 6, 95125 Catania, Italy
e-mail: sscire@unict.it

C. Bongiorno
Consiglio Nazionale delle Ricerche—Istituto per la Microelettronica e Microsistemi, Ottava Strada 5, Zona Industriale, 95121 Catania, Italy

the catalytically active species, stabilizing them against sintering [38]. The precursor used for catalyst preparation can also affect the dispersion and the metal size of the active species over the support [24, 39, 40].

Recently we found that Ru supported on an activated carbon of mineral origin is more active with respect to Ru on other supports, such as ceria, titania and alumina [24]. This behaviour was accounted for by the high surface area of the activated carbon and its high chemical inertness at high pH values. Moreover, results showed that on the investigated carbon the Ru precursor also affected the catalytic activity, with $RuCl_3$ resulting in better performance in terms of H_2 production rates with respect to $Ru(NO)(NO_3)_3$ [24]. Characterization data showed that the Ru particle size depended on the precursor used, with $Ru(NO)(NO_3)_3$ leading to much smaller Ru nanoparticles (average diameter <1 nm) compared to $RuCl_3$ (average diameter of 2.4 nm). It was suggested that the $NaBH_4$ hydrolysis on Ru/activated carbon is a structure sensitive reaction favored by larger Ru clusters, such as those formed on ex-$RuCl_3$ catalysts.

It is known that activated carbons can exhibit different chemical and morphological properties as a result of the origin and the preparation method [41]. On this basis, this work aimed to evaluate the effect of both the carbon origin (mineral or vegetable) and the Ru precursor ($RuCl_3$ or $Ru(NO)(NO_3)_3$) on $NaBH_4$ hydrolysis over Ru/carbon catalysts.

2 Experimental

The preparation of Ru/carbon catalysts (2 wt% Ru) was carried out by incipient wet impregnation of the support with an aqueous solution of the precursor, $RuCl_3$ from Sigma Aldrich or $Ru(NO)(NO_3)_3$ from Alfa Aesar. Two activated carbons were used as support, namely: (a) vegetable carbon (Sicarb, CA-SANSA), produced from exhausted olive husks, surface area: 1200 m^2g^{-1}; (b) mineral carbon (Carbonitalia Srl, E55), surface area: 650 m^2g^{-1}. Catalysts were coded as RuX/Y, where X is the Ru precursor used (N: $Ru(NO)(NO_3)_3$ and C: $RuCl_3$) and Y the activated carbon (M: mineral carbon and V: vegetable carbon). Two further catalysts were prepared by adding potassium to the mineral carbon (impregnation with KOH solution and subsequent treatment at 300 °C in He) prior to the impregnation with $RuCl_3$ (sample coded as RuC/M–K) or $Ru(NO)(NO_3)_3$ (RuN/M–K sample). It must be noted that the addition of Ru and/or K did not modify the surface area of carbon supports due to the low charge of the metal and the high surface area of the supports.

Activity measurements were carried out at atmospheric pressure in a 100 ml three-neck flask batch reactor, with a magnetic stirrer (300 rpm). Both the solution and the catalyst were admitted into the flask through the central neck, the two lateral ones were respectively used to connect the thermocouple monitoring the reaction temperature, and a gas flowmeter measuring the volume of H_2 evolved. Before reaching the flowmeter, the hydrogen passed through a steam trap containing anhydrous sodium sulphate in order to remove the water vapour. To rule out possible temperature effects due to the exothermicity of the reaction, experiments were carried out in isothermal conditions, maintaining the reaction temperature at a constant value (±0.3 °C) by circulation of an ethylene glycol/water solution in an external jacket connected with a thermostat. 10 wt% sodium borohydride solutions were prepared by dissolving sodium borohydride (Fluka, purity > 96%) into a 4 wt% NaOH solution. In a typical experiment the $NaBH_4$ solution (15 ml) was mixed with 25 ml of a 4 wt% NaOH water solution and then poured into the flask waiting until the temperature reached a constant value, then the catalyst (0.1 g, 14–20 mesh grain size) was added to the solution. The evolved hydrogen flow measured by a gas flowmeter was reported at standard temperature and pressure (STP) conditions. Catalytic activity was calculated in terms of H_2 yield, i.e. the ratio of the volume of hydrogen experimentally evolved and the theoretical volume obtainable on the basis of the reaction stoichiometry ($NaBH_4 + 2H_2O \rightarrow NaBO_2 + 4H_2$). Before catalytic experiments, Ru samples were always reduced in flowing hydrogen at 300 °C for 1 h. Preliminary runs carried out at different flow rates ruled out external diffusion limitations. The absence of internal diffusion was verified by experiments with different grain size powders. Under the experimental condition of this work, no hydrogen production was observed with the bare supports.

Surface area measurements were carried out using the BET nitrogen adsorption method with a Sorptomatic series 1990 (Thermo Quest). Test samples were previously outgassed (10^{-3} Torr) at 120 °C.

Transmission electron microscopy was carried out with a Jeol JEM model 2010 instrument. The powdered samples were ultrasonically dispersed in ethanol and a few droplets of the suspension were deposited on a Cu grid coated with a holey carbon film. After solvent evaporation, the specimens were introduced into the microscope column. The average Ru diameter (d_{TEM}) was calculated using the following formula: $d_{TEM} = \sum(n_i d_i)/n$, where d_i is the diameter of particle i and the index i is included from 1 and n (total number of Ru particles).

A ZEIS model LEO 1550, equipped with an EDX OXFORD 7426 instrument, was used to obtain EDX data. The analyses were done using primary electron energy of 20 keV.

3 Results

3.1 EDX Analysis of Activated Carbon Supports

EDX analysis of both vegetable (V) and mineral (M) carbons was carried out in order to highlight differences in the elemental composition of the two activated carbon supports. EDX spectra reported in Fig. 1 show signals deriving from the K orbital levels. The penetration thickness of the incident electron ray is similar for the two carbons (16.2 μm) considering that they have similar density values (0.42 g/cm^3). The elemental composition for each carbon by weight % with the relative standard deviations (σ) is shown in Table 1. Carbon and oxygen are the main elements (around 90 %), with the O/C ratio being higher on the vegetable carbon, due to the higher concentrations of oxygenated (carboxyl, carbonyl, hydroxyl) groups on this type of carbon [41]. The results of Fig. 1 and Table 1 illustrate other differences between the two carbons. In particular, a significant concentration of potassium (2.39 wt%) and small amounts of sodium (0.21 wt%) were found only in V and not in M. Moreover iron (1.51 wt%) and sulphur (0.36 wt%) were present only in M and silicon and aluminium were more abundant in M compared to V, whereas calcium was more abundant in V than in M.

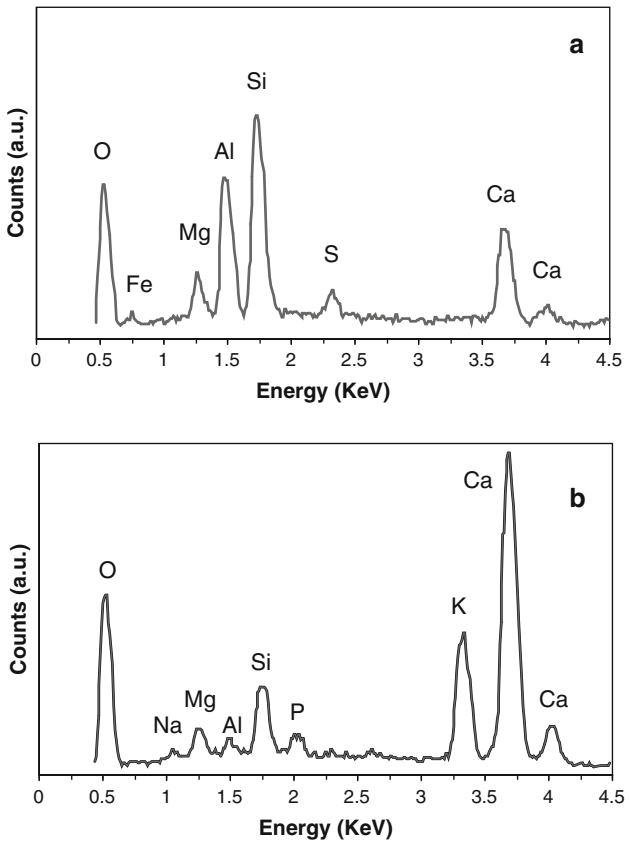

Fig. 1 EDX spectra of investigated supports. **a** M; **b** V. The signals due to carbon and oxygen below 0.4 keV are not shown in the figure due to their high intensity, which should mask the other elements

3.2 TEM Analysis and CO Chemisorption Data of Ru/C Catalysts

Figure 2 shows TEM microphotographs and the corresponding Ru size distributions of RuN/M (a, b), RuC/M (c, d), RuN/V (e, f) and RuC/V (g, h) catalysts. On all samples Ru metal particles appear homogeneously distributed on the carbon surface. The chemical nature of the dispersed nanoparticles was confirmed by the Fast Fourier Transformation (inset of Fig. 2a), showing diffraction rings (2.34, 2.13 and 2.05 Å) attributable to Ru with a hexagonal structure. From Fig. 2 and Table 2, where average Ru diameters estimated by TEM are summarized, it can be seen that both the support and the Ru precursor affect the size distribution of Ru particles. On each support, catalysts prepared from $RuCl_3$ have bigger Ru particles than those obtained using $Ru(NO)(NO_3)_3$ as the precursor. It is noteworthy that the above trend was confirmed by CO chemisorption experiments. Ru particle size estimated by chemisorption data was, in fact, in accordance with that obtained by TEM (Table 2).

3.3 Catalytic Activity and Kinetic Measurements

Figure 3 reports a comparison among the H_2 yield of investigated Ru/carbon catalysts as a function of reaction time for $NaBH_4$ hydrolysis carried out at 35 °C. From the figure it can be seen that the $NaBH_4$ hydrolysis activity was in the order: RuN/V > RuC/M > RuN/M > RuC/V. The good linearity in the first portion of the data of H_2 yield versus reaction time clearly demonstrates that $NaBH_4$ hydrolysis over Ru/carbon catalysts, under the experimental conditions employed is a zero order reaction with respect to $NaBH_4$. This is in accordance with reported data on other Ru/carbon samples under analogous reaction conditions (temperature and $NaBH_4$ concentration) [22, 24, 42]. On this basis, the kinetic parameters (kinetic constants and apparent activation energies) were calculated for each catalyst, measuring the H_2 yield vs. reaction time at four different temperatures. As a representative example, Fig. 4 shows data obtained at 15, 25, 35 and 45 °C on the most active sample, namely RuN/V. The results for all four investigated samples are summarized in Table 2. It is significant that activation energies range from 53.4 to 67 kJ mol^{-1}, values which are comparable with those reported in the literature on supported Ru catalysts [6, 7, 24, 43]. Finally, it must be underlined that the activity did not significantly change if the same batch of catalyst was reused, after filtration and washing with water, for three successive catalytic tests.

Table 1 Elemental composition of investigated carbons obtained by EDX (σ = relative standard deviation)

Element	Mineral carbon		Vegetable carbon	
	Weight (%)	σ	Weight (%)	σ
C	72.61	0.51	66.13	0.63
O	18.08	0.53	23.00	0.59
Na	Not present	–	0.21	0.05
Mg	0.59	0.05	0.43	0.04
Al	1.88	0.06	0.14	0.03
Si	2.76	0.07	0.89	0.05
P	Not present	–	0.30	0.04
S	0.36	0.04	Not present	–
K	Not present	–	2.39	0.07
Ca	2.21	0.07	6.51	0.13
Fe	1.51	0.10	Not present	–

4 Discussion

The catalytic results reported in the previous chapter showed that the activity of Ru/activated carbon catalysts depends both on the carbon type and the precursor used. When the mineral carbon was used as support, the sample prepared by $RuCl_3$ exhibited higher activity (higher kinetic constant and lower activation energy) compared to the corresponding sample prepared from $Ru(NO)(NO_3)_3$, whereas the reverse trend was found on the vegetable carbon supported system. Characterization data, namely TEM, CO chemisorption and EDX analysis, helped us to rationalize the above behaviour. In fact, TEM and CO chemisorption (Fig. 2 and Table 2), showed that on each carbon the size of Ru nanoparticles depends on the Ru precursor used: $Ru(NO)(NO_3)_3$ always resulting in smaller Ru nanoparticles compared to $RuCl_3$. The attainment of Ru catalysts with higher dispersion using $Ru(NO)(NO_3)_3$ has been reported in the literature in the case of ruthenium supported on various metal oxides (MgO, Al_2O_3, SiO_2, H-ZSM5 zeolite) [39, 40, 44–46]. It was proposed that polymeric hydroxy-species of Ru chloro-complexes are formed in $RuCl_3$ aqueous solutions, leading to large Ru particles upon reduction [45, 47]. Data in Table 2 also showed that the support concurs with the precursor to determine the Ru particle size. In fact, the mineral carbon leads to smaller Ru particles than the vegetable one, notwithstanding this latter having a much higher surface area (1200 vs. 650 m^2g^{-1}), which should instead favour the spreading of the active metal over the support surface. EDX analysis (Fig. 1 and Table 1) showed important differences in the elemental composition of the two investigated carbons, which can play a key role in affecting the formation of metal clusters during the catalyst preparation. In fact, the vegetable carbon exhibits significant amounts of alkali metals Na, and to a greater extent, K which are instead absent in the mineral one. According to the literature, it can be proposed that alkali metals cause the sintering of supported noble metal nanoparticles [48]. It must be underlined that the presence of chlorine deriving from the $RuCl_3$ precursor can boost this effect, acting in synergy with the alkali metals present on the support, thus resulting in very large Ru particles such as those found on the sample prepared by $RuCl_3$ on the carbon of vegetable origin (RuC/V). In order to verify this suggestion, we prepared two further catalysts where potassium was added to the mineral carbon prior to the impregnation with the Ru solution. The addition of K actually resulted in larger Ru particles than those formed on the K-free mineral carbon and the extent of this increase was larger on samples prepared by the Cl-containing Ru precursor (Table 2). It must be noted that catalytic data reported in Table 2 demonstrated that the addition of potassium to mineral carbon caused a decrease in the activity of the ex-$RuCl_3$ sample, whereas the opposite behaviour was observed on the ex-$Ru(NO)(NO_3)_3$ series. This result can be explained on the basis of the relationship found between kinetic constants of $NaBH_4$ hydrolysis and Ru particle diameters (Fig. 5). The figure in fact shows a typical volcano plot with a maximum of activity around 2.5 nm, confirming that $NaBH_4$ hydrolysis over Ru/carbon is a structure sensitive reaction [24] and, specifically, demonstrating that Ru nanoparticles with an optimal size are required. According to the literature [13, 22], active sites in $NaBH_4$ hydrolysis are made of ensembles of adjacent Ru atoms on which the reagent molecules (H_2O and $NaBH_4$) are co-adsorbed to form the activated complex, following the classical Langmuir–Hinshelwood model. This also agrees well with the observed zero-order of reaction in borohydride. Predictably, Ru particles which are too small do not allow the formation of the activated complex, whereas with Ru particles which are too large the probability of finding active sites strongly decreases. The occurrence of an optimal size (2 nm) has been already reported by Kojima

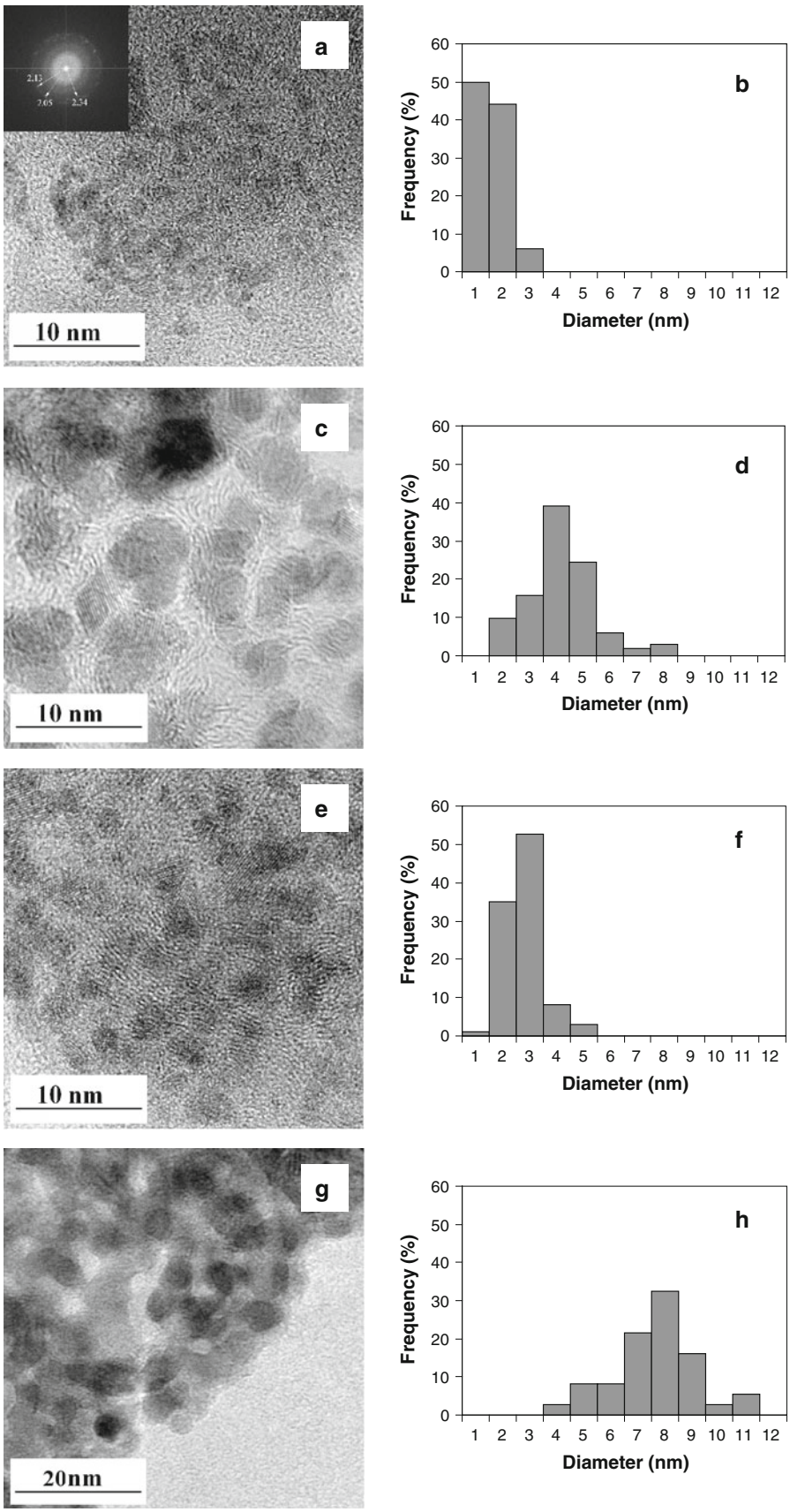

Fig. 2 TEM photographs (**a**, **c**, **e**, **g**) and Ru size distribution (**b**, **d**, **f**, **h**) of RuN/M (**a**, **b**); RuC/M (**c**, **d**); RuN/V (**e**, **f**); RuC/V (**g**, **h**)

Table 2 Kinetic data and average Ru size of Ru/carbon samples

Code	Ru diameter (nm)		K (L_{H2} g $^{-1}_{cat}$ min^{-1})				E_a (KJ mol^{-1})
	By TEM	By CO	15 °C	25 °C	35 °C	45 °C	
RuN/V	2.8	2.2	0.27	0.57	1.16	2.21	53.4
RuC/V	7.8	9.2	0.07	0.19	0.45	0.98	67.0
RuN/M	1.5	1.0	0.11	0.28	0.56	1.30	61.1
RuC/M	4.2	5.4	0.15	0.36	0.73	1.50	58.1
RuN/M–K	–	1.8	–	–	0.74	–	–
RuC/M–K	–	10.1	–	–	0.39	–	–

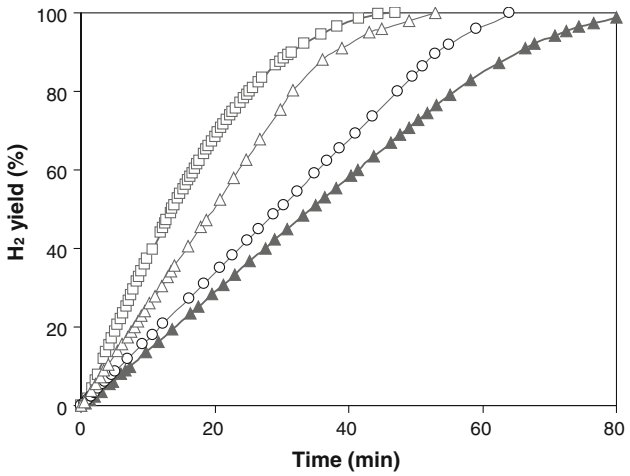

Fig. 3 H_2 yield as a function of reaction time over Ru/carbon catalysts. *Opened square* RuN/V; *opened triangle* RuC/M; *opened circle* RuN/M; *filled triangle* RuC/V. Experiments were carried out at T = 35 °C in isothermal conditions

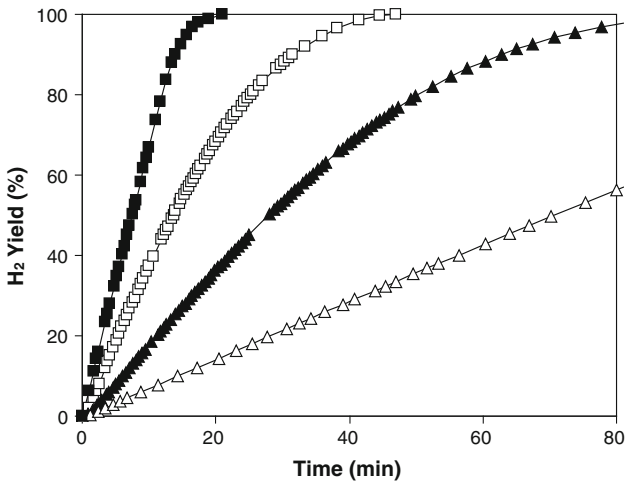

Fig. 4 H_2 yield as a function of reaction time at four different temperatures over RuN/V sample. *Filled square* 45 °C; *opened square* 35 °C; *filled triangle* 25 °C; *opened triangle* 15 °C

et al. using Pt/C catalysts [31]. Therefore it can be inferred that the choice of the most suitable activated carbon to be used as support of ruthenium for $NaBH_4$ hydrolysis over

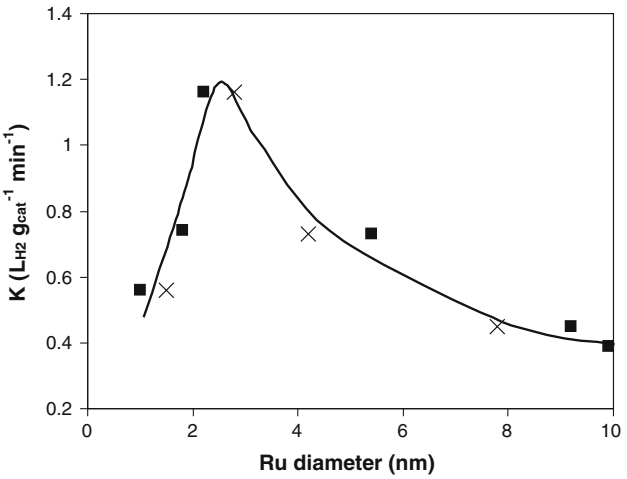

Fig. 5 Kinetic constants (calculated at 35 °C) versus Ru particle diameters estimated by: *multi symbol* TEM; *filled square* CO chemisorption

Ru/activated carbon catalysts is strictly related to that of the Ru precursor, in so far as the activated carbon type and the Ru precursor mutually affect the size of the Ru nanoparticles on the support, the best combination being that one resulting in Ru particles with diameters around 2.5 nm.

5 Conclusions

On the basis of the results reported in this paper the following conclusions can be drawn:

a) The size of Ru nanoparticles on investigated carbons depends on the Ru precursor used, with $Ru(NO)(NO_3)_3$ always resulting in smaller Ru nanoparticles compared to $RuCl_3$.
b) Support elemental composition also influences the metal particle size. The presence of alkali metals favours Ru sintering during the catalyst preparation.
c) The best combination of the carbon type and the Ru precursor is that leading to Ru particles with diameters around 2.5 nm, regarded as optimal for the $NaBH_4$ hydrolysis.

References

1. Lemons RA (1990) J Power Sources 29:251
2. Schlapbach L, Zuttel A (2001) Nature 414:353
3. Ross DK (2006) Vacuum 80:1084
4. Kong VCY, Foulkes FR, Kirk DW, Hinatsu JT (1999) Int J Hydrogen Energy 24:665
5. Aiello R, Sharp JH, Matthew MA (1999) Int J Hydrogen Energy 24:1123
6. Amendola SC, Sharp-Goldman SL, Janjua MS, Spencer NC, Kelly MT, Petillo PJ, Binder M (2000) Int J Hydrogen Energy 25:969
7. Amendola SC, Onnerud P, Kelly MT, Petillo PJ, Sharp-Goldman SL, Binder M (2000) J Power Sources 85:186
8. Wee JH, Lee KY, Kim SH (2006) Fuel Process Technol 87:811
9. Kojima Y, Kawai Y, Kimbara M, Nakanishi H, Matsumoto S (2004) Int J Hydrogen Energy 29:1213
10. Kojima Y, Kawai Y, Nakanishi H, Matsumoto S (2004) J Power Sources 135:36
11. Kojima Y, Suzuki K, Fukumoto K, Kawai Y, Kimbara M, Nakanishi H, Matsumoto S (2004) J Power Sources 125:22
12. Kim JH, Lee H, Han SC, Kim HS, Song MS, Lee JY (2004) Int J Hydrogen Energy 29:263
13. Liu BH, Li ZP (2009) J Power Sources 187:527
14. Kojima Y, Haga T (2003) Int J Hydrogen Energy 28:989
15. Atiyeh HK, Davis BR (2007) Int J Hydrogen Energy 32:229
16. Chen CW, Chen CY, Huang YH (2009) Int J Hydrogen Energy 34:2164
17. Schlesinger HI, Brown HC, Finholt AE, Gilbreath JR, Hoekstra HR, Hyde EK (1953) J Am Chem Soc 752:15
18. Demirci UB, Garin F (2008) J Mol Catal A 279:57
19. Gervasio D, Tasic S, Zenhausern F (2005) J Power Sources 149:15
20. Zhang Q, Smith GM, Wu Y (2007) Int J Hydrogen Energy 32: 4731
21. Zhang J, Fisher TS, Gore J, Hazra D, Ramachandran PV (2006) Int J Hydrogen Energy 31:2292
22. Zhang J, Delgass WN, Fisher TS, Gore JP (2007) J Power Sources 164:772
23. Zhang Q, Wu Y, Sun X, Ortega J (2007) Ind Eng Chem Res 46: 1120
24. Crisafulli C, Scirè S, Salanitri M, Zito R, Calamia S (2011) Int J Hydrogen Energy 36:3817
25. Lee J, Kong KY, Jung CR, Cho E, Yoon SP, Han J, Lee TG, Nam SW (2007) Catal Today 120:305
26. Jeong SU, Kim RK, Cho EA, Kim HJ, Nam SW, Oh IH, Hong SA, Kim SH (2005) J Power Sources 144:129
27. Jeong SU, Cho EA, Nam SW, Oh IH, Jung UH, Kim SH (2007) Int J Hydrogen Energy 32:1749
28. Ye W, Zhang HM, Xu DY, Ma L, Yi BL (2007) J Power Sources 164:544
29. Huang Y, Wang Y, Zhao R, Shen PK, Wei Z (2008) Int J Hydrogen Energy 33:7110
30. Liu BH, Li Q (2008) Int J Hydrogen Energy 33:7385
31. Kojima Y, Suzuki K, Fukumoto K, Sasaki M, Yamamoto T, Kawai Y, Hayashi H (2002) Int J Hydrogen Energy 27:1029
32. Wu C, Zhang HM, Yi BL (2004) Catal Today 93–95:477
33. Hua D, Hanxi Y, Xinping A, Chuansin C (2003) Int J Hydrogen Energy 28:1095
34. Pinto A, Falcao DS, Silva RA, Rangel CM (2006) Int J Hydrogen Energy 31:1341
35. Metin O, Ozkar S (2007) Int J Hydrogen Energy 32:1707
36. Patel N, Guella G, Kale A, Miotello A, Patton B, Zanchetta C, Mirenghi L, Rotolo P (2007) Appl Catal A 323:18
37. Patel N, Patton B, Zanchetta C, Fernandes R, Guella G, Kale A, Miotello A (2008) Int J Hydrogen Energy 33:287
38. Che M, Clause O, Marcilly CH (1999) In: Ertl G, Knözinger H, Weitkamp J (eds) Preparation of solid catalysts. Wiley-VCH, Weinheim, pp 315–340
39. Crisafulli C, Maggiore R, Scirè S, Solarino L (1990) J Mol Catal 63:55
40. Crisafulli C, Scirè S, Maggiore R, Minicò S, Galvagno S (1999) Catal Lett 59:21
41. Marsh H, Rodriguez-Reinoso F (2006) Activated carbons. Elsevier, Oxford
42. Shang Y, Chen R, Jiang G (2008) Int J Hydrogen Energy 33:6719
43. Park JH, Shakkthivel P, Kim HJ, Han MK, Jang JH, Kim YR et al (2008) Int J Hydrogen Energy 33:1845
44. Crisafulli C, Maggiore R, Scirè S, Galvagno S, Milone C (1993) J Mol Catal 83:237
45. Myeth JA, Schwarz JA (1989) J Catal 118:203
46. Hong AJ, Rouco AJ, Resasco DE, Haller GL (1987) J Phys Chem 91:2665
47. Rard JA (1985) Chem Rev 85:1
48. Satterfield CN (1991) Heterogeneous catalysis in industrial practice. McGraw-Hill, New York